Quantum Boltzmann equation for strongly correlated electrons

Antonio Picano, Jiajun Li, and Martin Eckstein
Department of Physics, University of Erlangen-Nürnberg, 91058 Erlangen, Germany

(Received 22 January 2021; revised 21 June 2021; accepted 29 June 2021; published 6 August 2021)

Collective orders and photoinduced phase transitions in quantum matter can evolve on timescales which are orders of magnitude slower than the femtosecond processes related to electronic motion in the solid. Quantum Boltzmann equations can potentially resolve this separation of timescales, but are often constructed by assuming the existence of quasiparticles. Here we derive a quantum Boltzmann equation which only assumes a separation of timescales (taken into account through the gradient approximation for convolutions in time), but is based on a nonperturbative scattering integral, and makes no assumption on the spectral function such as the quasiparticle approximation. In particular, a scattering integral corresponding to nonequilibrium dynamical mean-field theory is evaluated in terms of an Anderson impurity model in a nonequilibrium steady state with prescribed distribution functions. This opens the possibility to investigate dynamical processes in correlated solids with quantum impurity solvers designed for the study of nonequilibrium steady states.

DOI: 10.1103/PhysRevB.104.085108

I. INTRODUCTION

One of the biggest challenges in the theoretical description of quantum many-particle systems is to predict their nonequilibrium dynamics at long times after a perturbation. This would be essential for the understanding of nonequilibrium phenomena in complex solids [1,2], including photoinduced metal-insulator transitions and hidden phases with spin, orbital, charge, or superconducting order [3–9]. The evolution of the electronic structure in these situations is often intertwined with the dynamics of the crystal lattice, collective orders, or slow electronic variables such as nonthermal band occupations, which is orders of magnitude slower than intrinsic electronic processes such as the electron tunneling between atoms. Moreover, a large timescale separation becomes apparent in the thermalization of prethermal states [10–12], where approximate conservation laws provide a dynamical constraint [13,14].

A major goal is therefore to devise an approach that can explore the dynamics on the slower timescale, while still taking into account accurately the fast degrees of freedom. Within the Keldysh formalism, nonequilibrium quantum many-particle systems can be described in terms of time- and frequency-dependent spectral functions $A_{\boldsymbol{k}}(\omega, t)$ and distribution functions $F_{\boldsymbol{k}}(\omega, t)$. (For simplicity, spin and orbital indices in addition to momentum $\boldsymbol{k}$ are not shown here.) A large separation can become evident between the variation of the functions with time t, and the intrinsic timescales related to the linewidth of relevant spectral features. If these timescales are well separated, one can cast the full many-body dynamics into a differential equation known as the quantum Boltzmann equation (QBE) [15,16]. In abstract form, the QBE defines a scattering contribution to the evolution of the distribution functions

$$[\partial_t F_{\boldsymbol{k}}(\omega, t)]_{\text{scatt}} = I[F, A], \tag{1}$$

where the so-called scattering integral I depends on the spectrum and distribution function at the same time. The full time dependence is determined by additional contributions from the coherent single-particle propagation, and a separate equation for the evolution of the spectrum in terms of the distribution function.

One of the major challenges of developing a proper QBE has been an appropriate treatment of strong interactions, which play crucial roles in nuclear collisions, fluid dynamics, plasma dynamics, and in particular, strongly correlated solids. So far, generalized quantum kinetic equations have been developed along different pathways based on, e.g., reduced density operators and nonequilibrium Green's functions [17]. For the former approach, the non-Markovian Boltzmann equation is able to include many-body effects, such as quasiparticle damping and mass renormalization by means of the introduction of a suitable closure relation to the Bogolyubov-Born-Green-Kirkwood-Yvon (BBGKY) hierarchy of correlations [18]. In the context of solid-state physics, this formulation has recently been applied to the Fermi-Hubbard model to describe the dynamics of charge excitation in Mott insulators [19].

These developments, though capable of treating correlation effects, usually require the existence of well-defined quasiparticles. Within the QBE, the quasiparticle approximation assumes the spectra $A_{\boldsymbol{k}}(\omega, t)$ to be sharply peaked at energies $\omega = \epsilon_{\boldsymbol{k}}$, and therefore allows to evaluate the equation on shell, trading the frequency-dependent distribution function for quasiparticle occupations $n_{\boldsymbol{k}}(t)$. In solid-state systems, this approximation is accurate for semiconductors or Fermi liquids with well-defined quasiparticles [20], but it gets challenged in strongly correlated solid-state systems. For example, doped Mott insulators show strange metallic behaviors without well-defined Fermi-liquid quasiparticles in a wide

parameter regime [21,22], and similar behavior is observed in photodoped Mott insulators [23–27].

For that reason, the dynamics of correlated solid-state systems has been mostly discussed within the formally exact nonequilibrium Green's function (NEGF) techniques. In the NEGF formalism, the dynamics is described in terms of two-time Green's functions $G_{\boldsymbol{k}}(t,t')$, which are related to spectra and occupation functions through a Fourier transform with respect to relative time $t-t'$. A two-time self-energy acts as a memory kernel in a non-Markovian propagation of the Green's functions, the so-called Kadanoff-Baym equation. NEGF techniques can be combined with different diagrammatic approximations [28–31], including in particular dynamical mean-field theory (DMFT) [32,33], and they do not rely on a quasiparticle approximation for the spectrum. This enables us to investigate systems in the vicinity of the Mott insulator, where arbitrary high-order diagrams (at least in terms of the local Green's function) are needed, and so the approximations derived from the hierarchy of correlations (like the random phase approximation, or *GW* approximation) are not sufficient. On the other hand, NEGF techniques also do not make use of the timescale separation, and therefore imply a high numerical cost: The effort scales like $O(t_{\mathrm{max}}^3)$ with the simulation time t_{max}, as compared to $O(t_{\mathrm{max}})$ for the QBE.

For weakly interacting systems, generalized Kadanoff-Baym ansatz (GKBA) [34] has recently been set up to reach $O(t_{\mathrm{max}})$ scaling of the computational effort [35]. The GKBA is an NEGF-based method to derive the equation of motion for a time-dependent distribution function [34]. It is suitable for the case of weak scattering in the system, when the individual collisions are not very frequent, and the quasiparticle lifetime is long. The GKBA method has the advantage of reducing significantly the otherwise enormous computational demand requested by full NEGF simulations, while retaining a good accuracy as demonstrated in many benchmark calculations [36–38]. However, current implementations of the GKBA are based on diagrammatic approximations which fail to capture various many-body effects in strongly correlated systems, such as the Mott metal-insulator transition and strange metallic behavior. The main conceptual challenge against making use of the GKBA for such situations is that the approach requires an additional ansatz for the retarded propagator, which is often chosen to be a Hartree propagator [39]. For strongly correlated systems, systematic truncation [40] and compact compression [41] of the memory kernel in the Kadanoff-Baym equations provide a promising direction of reducing computational costs and reaching longer simulation times, while the investigation of many fundamental questions has still remained out of reach.

It would therefore be desirable to formulate a QBE which incorporates the simplifications due to the timescale separation, but does not rely on quasiparticle or perturbative approximations, for the description of the relaxation dynamics in strongly correlated systems in the vicinity of the Mott transition. In fact, it is crucial for our purposes to get rid of the quasiparticle approximation, and to evaluate the scattering kernel in a nonperturbative manner: The electronic structure in correlated solid-state systems depends strongly on the nonequilibrium distribution, as most clearly demonstrated through the possibility of photoinduced metal-insulator transitions. For example, if the equilibrium state of the system is described well by means of DMFT, the steady-state fixed point of the QBE should be identical to this DMFT solution. A previous work has successfully employed a QBE without the quasiparticle approximation for a Mott insulator [42,43], assuming a rigid density of states and a renormalized second-order scattering integral. Here we show how such a scattering integral can be obtained from an *auxiliary nonequilibrium steady-state formalism*. This allows to consistently combine the QBE with nonperturbative methods which have been developed to study true nonequilibrium steady states within DMFT [44–50].

The paper is organized as follows: In Sec. II, we present the formulation of a nonperturbative QBE which is consistent with nonequilibrium DMFT. In Sec. III we compare its solution to a nonequilibrium DMFT simulation for the thermalization in a correlated metal. Section IV gives a conclusion and outlook.

II. QUANTUM BOLTZMANN EQUATION

A. General setting

We will derive the QBE for a generic model,

$$H=\sum_{\boldsymbol{k},a,b} h_{\boldsymbol{k},ab}(t)c^{\dagger}_{\boldsymbol{k},a}c_{\boldsymbol{k},b}+H_{\mathrm{int}}, \tag{2}$$

where $c_{\boldsymbol{k},a}$ ($c^{\dagger}_{\boldsymbol{k},a}$) denotes the annihilation (creation) operator for a fermion with spin and orbital indices a and momentum $\boldsymbol{k}$, and H_{int} is an arbitrary two-particle interaction, and $h_{\boldsymbol{k},ab}(t)$ incorporates all single-particle terms. We assume that the system of interest is initially prepared in thermal equilibrium at temperature T, and driven out of equilibrium for times $t>0$ by external fields and a coupling to external heat and/or particle reservoirs. The description of this situation within many-body theory is based on contour-ordered Green's functions

$$G_{\boldsymbol{k},ab}(t,t')=-i\langle T_{\mathcal{C}}c_{\boldsymbol{k},a}(t)c^{\dagger}_{\boldsymbol{k},b}(t')\rangle, \tag{3}$$

with time arguments t and t' on the Keldysh contour $\mathcal{C}$ that runs from 0 to time t_{max} (the largest time of interest) on the real-time axis, back to 0, and finally to $-i\beta$ along the imaginary-time axis. (For an introduction to the Keldysh formalism and the notation, see, e.g., Ref. [32].) Spin and orbital indices will be no longer shown in the following for simplicity; all Green's functions, self-energies, dispersion functions $h_{\boldsymbol{k}}$ are matrices in these indices. From the contour-ordered function (3), one derives real- and imaginary-time Green's functions, of which the retarded, lesser, and greater components are most important in the following. The retarded Green's function (with real-time arguments)

$$G^{R}_{\boldsymbol{k}}(t,t')=-i\theta(t-t')\langle[c_{\boldsymbol{k}}(t),c^{\dagger}_{\boldsymbol{k}}(t')]_{+}\rangle \tag{4}$$

is related to the spectral function of the system, while the occupied and unoccupied density of states are extracted from

the lesser Green's function

$$G^<_{\boldsymbol{k}}(t,t') = +i\langle c^\dagger_{\boldsymbol{k}}(t')c_{\boldsymbol{k}}(t)\rangle, \tag{5}$$

$$G^>_{\boldsymbol{k}}(t,t') = -i\langle c_{\boldsymbol{k}}(t)c^\dagger_{\boldsymbol{k}}(t')\rangle, \tag{6}$$

so that

$$G^R_{\boldsymbol{k}}(t,t') = \theta(t-t')[G^>_{\boldsymbol{k}}(t,t') - G^<_{\boldsymbol{k}}(t,t')]. \tag{7}$$

In equilibrium, or in any time-translationally invariant state, all two-time correlation functions depend only on the relative time $t-t'$. By taking the Fourier transform of G^R with respect to this time difference, one obtains the spectral function A:

$$A_{\boldsymbol{k}}(\omega) = -\frac{1}{\pi}\mathrm{Im}G^R_{\boldsymbol{k}}(\omega + i0), \tag{8}$$

which is related to the lesser and greater Green's functions through a fluctuation-dissipation theorem

$$G^<_{\boldsymbol{k}}(\omega) = 2\pi i A_{\boldsymbol{k}}(\omega) f_\beta(\omega), \tag{9}$$

$$G^>_{\boldsymbol{k}}(\omega) = -2\pi i A_{\boldsymbol{k}}(\omega)[1 - f_\beta(\omega)], \tag{10}$$

where $f_\beta(\omega)$ is the Fermi distribution function, $f_\beta(\omega) = 1/(e^{\beta\omega}+1)$. In a nonequilibrium steady state, one can thus define the distribution function as the ratio

$$F_{\boldsymbol{k}}(\omega) = \frac{G^<_{\boldsymbol{k}}(\omega)}{2\pi i A_{\boldsymbol{k}}(\omega)}. \tag{11}$$

This is an energy distribution function, which is defined even in the absence of well-defined quasiparticles. The QBE provides an equation of motion for its time-dependent generalization, as introduced in the following.

B. The QBE

For every two-time quantity $X(t,t')$ one can introduce the Wigner transform

$$X(\omega,t) = \int ds\, e^{i\omega s} X(t+s/2, t-s/2), \tag{12}$$

where t is the average time and $s = t-t'$ is the relative time. In particular, this can be used to define a time-dependent spectrum and occupation function $F_{\boldsymbol{k}}(\omega,t)$ in analogy to Eqs. (7), (8), and (11):

$$A_{\boldsymbol{k}}(\omega,t) = -\frac{1}{\pi}\mathrm{Im}G^R_{\boldsymbol{k}}(\omega+i0,t) \tag{13}$$

$$= [G^>_{\boldsymbol{k}}(\omega,t) - G^<_{\boldsymbol{k}}(\omega,t)]/(-2\pi i), \tag{14}$$

$$F_{\boldsymbol{k}}(\omega,t) = G^<_{\boldsymbol{k}}(\omega,t)/[2\pi i A_{\boldsymbol{k}}(\omega,t)], \tag{15}$$

where $G^{R,<,>}_{\boldsymbol{k}}(\omega,t)$ are given by the Wigner transform.

While Eqs. (13)–(15) always provide a valid mathematical definition, the functions gain a physical significance in particular in the limit in which there is a well-defined separation of timescales. Let us assume that there are scales $\delta\omega$ and δt on which $G(\omega,t)$ varies in frequency and time, such that

$$\left|\frac{\partial_\omega G_{\boldsymbol{k}}(\omega,t)}{G_{\boldsymbol{k}}(\omega,t)}\right| < 1/\delta\omega, \quad \left|\frac{\partial_t G_{\boldsymbol{k}}(\omega,t)}{G_{\boldsymbol{k}}(\omega,t)}\right| < 1/\delta t \tag{16}$$

for lesser, greater, or retarded components. The scale $\delta\omega$ measures the relevant internal energy differences in the system, such as the linewidth of relevant spectral features, and δt sets the scale for the time evolution, with $\delta t \to \infty$ in a steady state. The QBE will be derived in the limit where these timescales are well separated,

$$\delta t \gg 1/\delta\omega. \tag{17}$$

Practically, one makes an estimation *a priori* of $\delta\omega$ and δt and then checks, *a posteriori*, that the time constants of the exponential relaxation of relevant quantities, like the energy, are indeed much greater than $1/\delta\omega$, where $\delta\omega$ can be extracted, e.g., from the linewidth of the quasiparticle peak. Equation (17) represents also the limit in which the spectral and occupation functions gain their usual meaning in terms of a density of states: One can always approximate $G(\omega,t)$ by the average

$$G(\omega,t) \approx \int \frac{dt'd\omega'}{\pi\Omega\tau} e^{-(\frac{t'}{\tau})^2-(\frac{\omega'}{\Omega})^2} G(\omega+\omega', t+t') \tag{18}$$

over a time interval $\tau \ll \delta t$ and a frequency interval $\Omega \ll \delta\omega$ on which the function varies weakly; τ and Ω represent the smallest time and frequency windows for sampling the quantity of interest, e.g., the photoemission spectrum. With a sufficiently large timescale separation (17), it is possible to choose $\Omega = 1/\tau$ without violating the conditions $\tau \ll \delta t$ and $\Omega \ll \delta\omega$. With this, the average (18), with G replaced by $-iG^<$, is the expression for the time-resolved photoemission spectrum [51,52], computed with a Gaussian probe pulse of duration τ and spectral resolution $\Omega = 1/\tau$, and therefore has a well-defined interpretation in terms of an occupied density of states. In addition, this implies that the expression is real and positive, which can be proven by casting Eq. (18) in the form of a complete square using a Lehmann representation for the Green's function. In the same way, $iG^>(\omega,t)$ can be interpreted as the unoccupied density of states (electron addition spectrum), and the spectral function $A(\omega,t) = [G^>(\omega,t) - G^<(\omega,t)]/(-2\pi i)$ has the usual meaning of a single-particle density of states in the many-body system. Furthermore, we remark that by choosing $\Omega = 1/\tau$ we never violate the uncertainty principle since $\Omega\tau = 1$ ($\hbar = 1$).

The QBE provides an equation of motion for the spectral and occupation functions (13) and (15) in the limit of well-separated times [16]. Most importantly, the limit (17) allows for the simplification of the convolution $[A*B](t,t') = \int d\bar{t}\, A(t,\bar{t})B(\bar{t},t')$ of two real-time functions A and B. In mathematical terms, the Wigner transform of the convolution is given by the Moyal product

$$[A*B](\omega,t) = e^{\frac{i}{2}[\partial_t^A\partial_\omega^B - \partial_t^B\partial_\omega^A]} A(\omega,t)B(\omega,t). \tag{19}$$

If Eqs. (16) and (17) hold for A and B, the Moyal product can be simplified by considering only the leading term

$$[A*B](\omega,t) \approx A(\omega,t)B(\omega,t) \tag{20}$$

because $|\partial_t A\, \partial_\omega B| \ll |AB|$. This is the so-called *gradient approximation*. In a time-evolving state, Eq. (9) is generalized to the ansatz

$$G^<_{\boldsymbol{k}}(t,t') = \left[F_{\boldsymbol{k}} * G^A_{\boldsymbol{k}}\right](t,t') - \left[G^R_{\boldsymbol{k}} * F_{\boldsymbol{k}}\right](t,t'), \tag{21}$$

where $F_{\boldsymbol{k}}(t,t')$ depends on two times, and $G^A_{\boldsymbol{k}}(t,t') = G^R_{\boldsymbol{k}}(t',t)^\dagger$ is the advanced Green's function. By applying the gradient approximation (20) to this ansatz, we obtain the factorization

$$G^<_{\boldsymbol{k}}(\omega,t) = 2\pi i A_{\boldsymbol{k}}(\omega,t) F_{\boldsymbol{k}}(\omega,t), \tag{22}$$

equivalent to Eq. (15), using $G^A_{\boldsymbol{k}}(\omega,t) = G^R_{\boldsymbol{k}}(\omega,t)^\dagger$. We note that, in general, Eq. (22) can violate the causal structure of the Kadanoff-Baym differential equations [34]. Our approximation is nevertheless controlled by the separation of timescales, which will be tested in Sec. III D, and leads to a well-defined time-evolution scheme within this approximation.

In order to derive the QBE for the evolution of the distribution function $F_{\boldsymbol{k}}$, one can consider the equations of motion for the Green's function. For a noninteracting system with Green's function $\mathcal{G}_{\boldsymbol{k}}(t,t') = -i\langle \mathcal{T}_{\mathcal{C}} c_{\boldsymbol{k}}(t) c^\dagger_{\boldsymbol{k}}(t')\rangle$ this is written as

$$\left\{\mathcal{G}^{-1}_{\boldsymbol{k}} * \mathcal{G}_{\boldsymbol{k}}\right\}(t,t') = \delta_{\mathcal{C}}(t,t'), \tag{23}$$

$$\mathcal{G}^{-1}_{\boldsymbol{k}}(t,t') = [i\partial_t + \mu - h_{\boldsymbol{k}}(t)]\delta_{\mathcal{C}}(t,t'), \tag{24}$$

where $\delta_{\mathcal{C}}(t,t')$ represents the delta function on the Keldysh contour and μ is the chemical potential of the system. In the following, it will be convenient to also include the Hartree and Fock self-energies into the dispersion $h_{\boldsymbol{k}}(t)$. To include correlations we take into account the contour-ordered self-energy $\Sigma(t,t')$ and obtain the interacting Green's function G via the Dyson equation

$$\{[(\mathcal{G}_{\boldsymbol{k}})^{-1} - \Sigma_{\boldsymbol{k}}] * G_{\boldsymbol{k}}\}(t,t') = \delta_{\mathcal{C}}(t,t') \tag{25}$$

on the Keldysh contour. From the Dyson equation for the lesser component, $[(\mathcal{G}^R_{\boldsymbol{k}})^{-1} - \Sigma^R_{\boldsymbol{k}}] * G^<_{\boldsymbol{k}} = \Sigma^<_{\boldsymbol{k}} * G^A_{\boldsymbol{k}}$, and the ansatz (21), we get

$$\begin{aligned}\left(\mathcal{G}^R_{\boldsymbol{k}}\right)^{-1} * F_{\boldsymbol{k}} - F_{\boldsymbol{k}} * \left(\mathcal{G}^A_{\boldsymbol{k}}\right)^{-1} \\ = \Sigma^<_{\boldsymbol{k}} + \Sigma^R_{\boldsymbol{k}} * F_{\boldsymbol{k}} - F_{\boldsymbol{k}} * \Sigma^A_{\boldsymbol{k}}.\end{aligned} \tag{26}$$

(Real-time arguments are shown only where otherwise ambiguous.) We thus obtain the equation of motion for $F_{\boldsymbol{k}}(t,t')$:

$$\begin{aligned}i(\partial_t + \partial_{t'})F_{\boldsymbol{k}}(t,t') = h_{\boldsymbol{k}}(t)F_{\boldsymbol{k}}(t,t') - F_{\boldsymbol{k}}(t,t')h_{\boldsymbol{k}}(t') \\ + \Sigma^<_{\boldsymbol{k}} + \Sigma^R_{\boldsymbol{k}} * F_{\boldsymbol{k}} - F_{\boldsymbol{k}} * \Sigma^A_{\boldsymbol{k}}.\end{aligned} \tag{27}$$

Equation (27) is still exact. To obtain the QBE, we then use the gradient approximation (20) to rewrite Eq. (27) as

$$\partial_t F_{\boldsymbol{k}}(\omega,t) = -i[h_{\boldsymbol{k}}(t), F_{\boldsymbol{k}}(\omega,t)] + I_{\boldsymbol{k}}(\omega,t), \tag{28}$$

$$\begin{aligned}I_{\boldsymbol{k}}(\omega,t) = -i\big[\Sigma^R_{\boldsymbol{k}}(\omega,t)F_{\boldsymbol{k}}(\omega,t) - F_{\boldsymbol{k}}(\omega,t)\Sigma^A_{\boldsymbol{k}}(\omega,t) \\ + \Sigma^<_{\boldsymbol{k}}(\omega,t)\big],\end{aligned} \tag{29}$$

where $I_{\boldsymbol{k}}(\omega,t)$ is the *scattering integral*. This equation is completed by the Dyson equation for the retarded Green's function to leading order in the gradient approximation

$$G^R_{\boldsymbol{k}}(\omega,t) = \left[\omega + i0 + \mu - h_{\boldsymbol{k}}(t) - \Sigma^R_{\boldsymbol{k}}(\omega,t)\right]^{-1}. \tag{30}$$

This set of equations must be combined with a given expression for the self-energy. For example, a simple perturbative expression would be a second-order diagram in terms of a two-particle density-density interaction $v_{\boldsymbol{q}}$:

$$\Sigma_{\boldsymbol{k}}(t,t') = \sum_{\boldsymbol{k}',\boldsymbol{q}} v^2_{\boldsymbol{q}} G_{\boldsymbol{k}'+\boldsymbol{q}}(t,t')G_{\boldsymbol{k}'}(t',t)G_{\boldsymbol{k}'-\boldsymbol{q}}(t,t'). \tag{31}$$

Such an analytic perturbative expression for Σ can then be evaluated in the gradient approximation, thus closing the equation. In the following, we discuss a strategy to incorporate a nonperturbative self-energy approximation like DMFT into the QBE formalism, in which an explicit analytical expression for Σ is not given.

C. Nonperturbative evaluation of the scattering integral

In general, the self-energy includes contributions from the interaction, and a possible coupling to a noninteracting environment, which can be used to represent thermal and particle reservoirs [32,53,54]. In the following, we write $\Sigma = \Sigma_{\rm int} + \Gamma$, where $\Sigma_{\rm int}$ is the interaction contribution, and Γ represents the noninteracting reservoirs. Evaluating the interaction self-energy is the main challenge. We assume that the interaction self-energy $\Sigma_{\rm int}(t,t') = \hat{\Sigma}^{\rm skel}_{\boldsymbol{k},t,t'}[G]$ is a functional of the full Green's function G, as obtained in particular as the so-called skeleton expansion through derivatives of the Luttinger-Ward functional [55] for any conserving approximation [56]. DMFT and its extensions can be cast in this language [33]. A simple perturbative example would be the second-order diagram, Eq. (31). (For the application to DMFT below, Σ will be given in terms of the noninteracting impurity Green's function $\mathcal{G}$, which however itself is determined by G through the self-consistency.) Let us now imagine a system which has the same interaction but general noninteracting reservoirs so that the system resides in a nonequilibrium steady state (NESS) with steady-state spectrum $\bar{A}_{\boldsymbol{k}}(\omega)$, and the steady-state distribution $\bar{F}_{\boldsymbol{k}}(\omega)$. Evaluation of the full skeleton functional $\hat{\Sigma}^{\rm skel}_{\boldsymbol{k},t,t'}[G]$ at the translationally invariant Green's function $\bar{G}[\bar{A},\bar{F}]$ defines a nonequilibrium steady-state functional through the Wigner transform (12):

$$\hat{\Sigma}^{\rm NESS\text{-}skel}_{\boldsymbol{k},\omega}[\bar{A},\bar{F}] = \int ds\, e^{i\omega s}\, \hat{\Sigma}^{\rm skel}_{\boldsymbol{k},s/2,-s/2}[\bar{G}]. \tag{32}$$

This skeleton functional is universal in the sense that it parametrically depends only on the interaction [57], but not on the single-particle part of the Hamiltonian, and hence the functional (32) is independent of the choice of the reservoirs. In order to write the equations below in a more compact form, we note that the self-consistent evaluation of the functional (32), together with the steady-state Dyson equation for the retarded function

$$\bar{A}_{\boldsymbol{k}}(\omega) = -\frac{1}{\pi}\mathrm{Im}\frac{1}{\omega^+ + \mu - \bar{h}_{\boldsymbol{k}} - \bar{\Gamma}^R_{\boldsymbol{k}}(\omega) - \bar{\Sigma}^R_{{\rm int},\boldsymbol{k}}(\omega)} \tag{33}$$

and given $\bar{h}_{\boldsymbol{k}}$ and $\bar{\Gamma}^R_{\boldsymbol{k}}(\omega)$, implicitly defines a steady-state functional of the self-energy and the spectral function in terms of the distribution function only, which we will denote by

$$\hat{\Sigma}^{\rm NESS}_{\boldsymbol{k},\omega}\left[\bar{F};\bar{h}_{\boldsymbol{k}},\bar{\Gamma}^R_{\boldsymbol{k}}\right], \quad \hat{A}^{\rm NESS}_{\boldsymbol{k},\omega}\left[\bar{F};\bar{h}_{\boldsymbol{k}},\bar{\Gamma}^R_{\boldsymbol{k}}\right]. \tag{34}$$

Back to the QBE: at each order of a diagrammatic expression, the two-time self-energy $\Sigma_{\rm int}(t,t')$ can be written as a sum of convolutions and products of the full Green's

function G. In each of these terms, one can consistently use the leading order of the gradient approximation, in combination with the factorization (22). This procedure would be the same as evaluating $\hat{\Sigma}^{\rm skel}_{{\rm int},\boldsymbol{k},t,t'}[\bar{G}]$ with a time-translationally invariant function $\bar{G}$ with spectral function $\bar{A}_{\boldsymbol{k}}(\omega) = A_{\boldsymbol{k}}(\omega, t)$ and distribution function $\bar{F}_{\boldsymbol{k}}(\omega) = F_{\boldsymbol{k}}(\omega, t)$. Hence, the self-energy in the gradient approximation amounts to evaluating the NESS functional (32):

$$\Sigma_{{\rm int},\boldsymbol{k}}(\omega, t) = \hat{\Sigma}^{\text{skel-NESS}}_{\boldsymbol{k},\omega}[A(\cdot, t), F(\cdot, t)]. \tag{35}$$

Here the notation $X(\cdot, t)$ of the functional arguments $X = A, F$ indicates that the latter are considered as function of all their arguments except for t, which is considered as a fixed parameter. With Eq. (34), the QBE is now formally written as

$$\partial_t F_{\boldsymbol{k}}(\omega, t) = -i[h_{\boldsymbol{k}}(t), F_{\boldsymbol{k}}(\omega, t)] + I_{\boldsymbol{k},\omega}[F(\cdot, t)], \tag{36}$$

$$I_{\boldsymbol{k},\omega}[F(\cdot, t)] = -i\big[\Sigma^R_{\boldsymbol{k}}(\omega, t)F_{\boldsymbol{k}}(\omega, t) - F_{\boldsymbol{k}}(\omega, t)\Sigma^A_{\boldsymbol{k}}(\omega, t) + \Sigma^<_{\boldsymbol{k}}(\omega, t)\big], \tag{37}$$

where in the second line $\Sigma = \Sigma_{\rm int} + \Gamma$, with

$$\Sigma_{{\rm int},\boldsymbol{k}}(\omega, t) = \hat{\Sigma}^{\rm NESS}_{\boldsymbol{k},\omega}\big[F(\cdot, t); h_{\boldsymbol{k}}(t), \Gamma^R_{\boldsymbol{k}}(\cdot, t)\big]. \tag{38}$$

In addition, the spectral function is given by

$$A_{\boldsymbol{k}}(\omega, t) = \hat{A}^{\rm NESS}_{\boldsymbol{k},\omega}\big[F(\cdot, t); h_{\boldsymbol{k}}(t), \Gamma^R_{\boldsymbol{k}}(\cdot, t)\big]. \tag{39}$$

Physically, the last equation (39) means that we allow the electronic distribution function to instantaneously influence the electronic structure of the material. We will therefore refer to Eq. (39) as the *instantaneous response approximation*.

Equations (36)–(39) now provide a closed set of time-dependent equations. This implicit scheme allows a nonperturbative evaluation of the QBE, provided that an efficient numerical description of a NESS is available: To evaluate $\hat{\Sigma}^{\rm NESS}_{\boldsymbol{k},\omega}[F(\cdot, t), ...]$ and $A_{\boldsymbol{k}}(\omega, t) = \hat{A}^{\rm NESS}_{\boldsymbol{k},\omega}[F(\cdot, t), ...]$ for a given distribution function $\bar{F}$, we choose an *auxiliary steady-state system* with reservoir self-energy $\bar{\Gamma}^R_{\boldsymbol{k}}(\omega) = \Gamma^R_{\boldsymbol{k}}(\omega, t)$, while the bath occupation function, and hence $\bar{\Gamma}^<_{\boldsymbol{k}}(\omega)$, is treated as a free parameter. The latter is chosen such that the solution $\bar{F}_{\boldsymbol{k}}(\omega)$ gives the prescribed $F_{\boldsymbol{k}}(\omega, t)$, after which the outcomes $\bar{A}_{\boldsymbol{k}}(\omega)$ and $\bar{\Sigma}_{{\rm int},\boldsymbol{k}}(\omega)$ are used to evaluate (38) and (39). In particular, within nonequilibrium DMFT, where only local self-energies need to be evaluated in a quantum impurity model, several promising nonperturbative techniques are available that can directly target such nonequilibrium states (see discussion in Sec. IV). Once Eqs. (38) and (39) can be evaluated for a given F, the QBE equation (36) can be solved as any differential equation. (In the implementation below, we use a simple Runge-Kutta algorithm.)

In the following two sections, we will adapt the general QBE formalism to the nonequilibrium DMFT framework. Before that, we conclude this section with a side remark: It is known even in equilibrium that the self-consistent solution of the Dyson equation with a skeleton self-energy functional can have multiple unphysical solutions [58]. However, a possible multivaluedness of the functional (34) will not be a problem here. The functions $A_{\boldsymbol{k}}(\omega, t)$, $F_{\boldsymbol{k}}(\omega, t)$, and $\Sigma_{\boldsymbol{k}}(\omega, t)$ evolve continuously as a function of time, so that even if unphysical steady-state solutions exist for a given distribution function, the physical solution is always selected by the requirement of continuity and the initial condition. On the other hand, if the system would evolve as a function of time into a branching point where multiple solutions of Eq. (34) meet, this would hint at a rather unconventional dynamical behavior. For example, in equilibrium it is known that the multivaluedness of self-consistent perturbation theory is related to vertex singularities [59], and in the Hubbard model these vertex singularities apparently fall together with the dynamical critical point found in Ref. [60].

D. Scattering integral in DMFT

Within DMFT, one maps the lattice model (2) onto an effective single-site impurity model. The impurity site has the same interaction as a site in the lattice, and its coupling to the environment is described by the so-called *hybridization* function $\Delta(t, t')$, which is self-consistently determined such that the local ($\boldsymbol{k}$-averaged) lattice Green's function

$$G_{\rm loc}(t, t') = \sum_{\boldsymbol{k}} G_{\boldsymbol{k}}(t, t') \tag{40}$$

coincides with the impurity Green's function. The key approximation of DMFT is that the lattice self-energy is local in space (independent of $\boldsymbol{k}$), and one requires the local lattice self-energy to be identical to the impurity self-energy. In detail, the impurity model is defined by an action

$$\mathcal{S} = -i\int_{\mathcal{C}} dt\, H_{\rm loc}(t) - i\int_{\mathcal{C}} dt\, dt' \sum_{\sigma} c^\dagger_\sigma(t)\Delta(t, t')c_\sigma(t'), \tag{41}$$

in terms of the self-consistent hybridization function. The noninteracting Green's function $\mathcal{G}$ is determined by the Dyson equation

$$\mathcal{G}^{-1}(t, t') = [i\partial_t + \mu - h(t)]\delta_{\mathcal{C}}(t, t') - \Delta(t, t'), \tag{42}$$

where $h(t)$ is the single-particle Hamiltonian in the impurity model. The interacting impurity Green's function is given by

$$G^{-1}_{\rm imp} = \mathcal{G}^{-1} - \Sigma_{\rm imp}, \tag{43}$$

and the self-consistency requires

$$G_{\rm imp} = G_{\rm loc}, \quad \Sigma_{\rm imp} = \Sigma. \tag{44}$$

The self-consistent impurity model provides an implicit way to evaluate a nonperturbative expression $\hat{\Sigma}_{\rm int}[G_{\rm loc}]$ for a local self-energy in terms of a local Green's function. Along the line of the previous section, we can therefore use an impurity model in a NESS to construct the steady-state functional (38) for the local self-energy. An impurity model in the steady state simply implies that the hybridization function itself is translationally invariant in time, and is specified through its retarded and lesser components $\Delta^R(\omega)$ and $\Delta^<(\omega)$.

The evaluation of the functionals (38) and (39) within DMFT, for a given distribution function $\bar{F}_{\boldsymbol{k}}(\omega)$, depends on the type of impurity solver. Below we exemplify this for an impurity solver which determines the self-energy from an expansion in terms of the noninteracting impurity Green's function $\bar{\mathcal{G}}$ (such as weak-coupling Keldysh quantum Monte Carlo or iterated perturbation theory):

(1) Start with some guess for $\bar{\Sigma}^R_{\rm int}(\omega)$ and $\bar{\Sigma}^<_{\rm int}(\omega)$, and calculate the $\boldsymbol{k}$-dependent lattice Green's functions [Eq. (30) with $\boldsymbol{k}$-independent self-energy]

$$\bar{G}^R_{\boldsymbol{k}}(\omega) = \left[\omega + \mu - \bar{h}_{\boldsymbol{k}} - \bar{\Gamma}^R_{\boldsymbol{k}}(\omega) - \bar{\Sigma}^R_{\rm int}(\omega)\right]^{-1} \tag{45}$$

and the spectrum $\bar{A}_{\boldsymbol{k}}(\omega) = -\frac{1}{\pi}{\rm Im}G^R_{\boldsymbol{k}}(\omega + i0)$.

(2) Determine the lesser Green's function from the given distribution function

$$\bar{G}^<_{\boldsymbol{k}}(\omega) = 2\pi i \bar{F}_{\boldsymbol{k}}(\omega)\bar{A}_{\boldsymbol{k}}(\omega). \tag{46}$$

(3) Calculate the local lattice Green's functions

$$\bar{G}^{R,<}_{\rm loc}(\omega) = \sum_{\boldsymbol{k}} \bar{G}^{R,<}_{\boldsymbol{k}}(\omega, t). \tag{47}$$

(4) Express the noninteracting Green's function $\mathcal{G}$ of the impurity model in terms of $\Sigma_{\rm imp}$ of $G_{\rm imp}$ using the Dyson equation for the impurity model [Eqs. (42) and (43)] in the steady state. For example, this can be written as

$$\mathcal{G}^R(\omega) = \left[G^R_{\rm imp}(\omega)^{-1} + \Sigma^R_{\rm imp}(\omega)\right]^{-1}, \tag{48}$$

$$\Delta^<(\omega) = G^R_{\rm imp}(\omega)^{-1}G^<_{\rm imp}(\omega)G^A_{\rm imp}(\omega)^{-1} - \Sigma^<_{\rm imp}(\omega), \tag{49}$$

$$\mathcal{G}^<(\omega) = \mathcal{G}^R(\omega)\Delta^<\mathcal{G}^A(\omega), \tag{50}$$

Solve these equations for $\mathcal{G}(\omega)$ using the DMFT self-consistency for the lattice and impurity quantities $\Sigma_{\rm imp}(\omega) = \bar{\Sigma}_{\rm int}(\omega)$ and $G_{\rm imp}(\omega) = \bar{G}_{\rm loc}(\omega)$.

(5) Calculate a new $\Sigma_{\rm imp}$ by using an expansion in $\mathcal{G}^R(\omega)$.

(6) Set $\bar{\Sigma}^{R,<}_{\rm int}(\omega) = \Sigma^{R,<}_{\rm imp}(\omega)$, and iterate steps (2) to (5) until convergence.

This iteration is basically a steady-state nonequilibrium DMFT simulation where the distribution function of the system is prescribed and the distribution of the reservoirs is determined, in contrast to conventional steady-state DMFT where the distribution function of the system is determined by reservoirs with a given distribution function.

III. COMPARISON TO THE FULL DMFT SIMULATION

A. Model

As a first test case for the methodology, we study the particle-hole-symmetric single-band Hubbard model

$$\hat{H} = -t_h \sum_{\langle i,j\rangle,\sigma} c^\dagger_{i\sigma}c_{j\sigma} + U\sum_j \left(\hat{n}_{j\uparrow} - \tfrac{1}{2}\right)\left(\hat{n}_{j\downarrow} - \tfrac{1}{2}\right). \tag{51}$$

Here $c_{j,\sigma}$ denotes the annihilation operator for a fermion with spin $\sigma \in \{\uparrow, \downarrow\}$ at lattice site j, $\hat{n}_{j\sigma} = c^\dagger_{j\sigma}c_{j\sigma}$ is the particle-number operator, t_h the hopping matrix element between nearest-neighbor sites, and U the onsite interaction strength. The actual simulations assume a semielliptic local density of states $D(\epsilon) = \sqrt{4-\epsilon^2}/(2\pi)$ for the noninteracting model with bandwidth 4, corresponding to a Bethe lattice with hopping $t_h = 1$. The latter sets the unit of energy, and its inverse defines the unit of time ($\hbar = 1$).

The system is studied in the metallic regime, where U is smaller than the bandwidth. Initially, the system is in equilibrium with a inverse temperature β. Within a short time interval, we then create a nonthermal population of electrons and holes similar to a photoexcited population (the precise protocol is given below). This nonthermal population will then relax under the influence of the electron-electron interaction and the coupling to a phonon bath, and we compare a simulation of this relaxation dynamics within the full nonequilibrium DMFT simulation and the QBE.

For the excitation, we shortly couple a fermionic reservoir with density of states

$$A_{\rm bath}(\omega) = A(\omega - 2.5) + A(\omega + 2.5) \tag{52}$$

consisting of two smooth bands with bandwidth $W_{\rm bath} = 6$ around the energies $\omega = \pm 2.5$; we choose $A(\omega) = \frac{1}{\pi}\cos^2(\pi\omega/W_{\rm bath})$ in the interval $[-W_{\rm bath}/2, W_{\rm bath}/2]$ [see dashed line at the bottom of Fig 1(c) for $A_{\rm bath}(\omega)$]. Choosing a population inversion in this reservoir will lead to a rapid transfer of electrons from the system into the negative-energy part of the reservoir, and of electrons from the positive-energy part of the bath to the system, thus generating an electron transfer similar to a photoexcitation process. The bath adds a local contribution $\Gamma(t,t')$ to the self-energy (as obtained by integrating out the bath)

$$\Gamma(t,t') = V(t)G_{\rm bath}(t,t')V(t')^*, \tag{53}$$

where $V(t)$ is the time profile of the coupling, and $G_{\rm bath}(t,t')$ is the bath Green's function

$$G^R_{\rm bath}(t,t') = -i\theta(t-t')\int d\omega\, e^{-i\omega(t-t')}A_{\rm bath}(\omega), \tag{54}$$

$$G^<_{\rm bath}(t,t') = i\int d\omega\, e^{-i\omega(t-t')}f_{\rm bath}(\omega)A_{\rm bath}(\omega). \tag{55}$$

The bath occupation $f_{\rm bath}(\omega) = f_{-\beta}(\omega)$ is taken to be, during the whole time evolution of the system, a negative-temperature Fermi-Dirac distribution (population inversion), and the switching profile $V(t) = 0.75\,\sin^2[\pi/5(t-t_0)]$ is centered around an early time $t_0 = 27.5$ with a duration of just five inverse hoppings. In general, the QBE is expected to describe the evolution of the system only on timescales much longer than the inverse hopping, so that these details of the excitation protocol are not important for this study. Indeed, the signature of the specific excitation protocol is often wiped out by the fast electronic dynamics in solid-state systems, while we concentrate here on the slow evolution which can be described by the QBE.

The coupling to the bosonic bath is included via a local electron-phonon self-energy $\Sigma_{\rm ph}$. In order for the bosons to act as heat bath, we need to neglect the back action of the electrons on the phonons, and we take $\Sigma_{\rm ph}$ to be the simple first-order diagram of a local electron-phonon interaction

$$\Sigma_{\rm ph}(t,t') = g^2 G(t,t')D_{\rm ph}(t,t'), \tag{56}$$

where G is the fully interacting local electron Green's function of the system, g measures the electron-phonon coupling strength, and $D_{\rm ph}$ is the propagator for free bosons with an Ohmic density of states $\frac{\omega}{4\omega^2_{\rm ph}}\exp(-\omega/\omega_{\rm ph})$ with exponential cutoff $\omega_{\rm ph} = 0.2$. The occupation function of bosons is kept in equilibrium with inverse temperature β. The temperature of the heat bath is the same as the initial one of the system in equilibrium, such that the system will eventually thermalize back to its initial temperature long after the excitation.

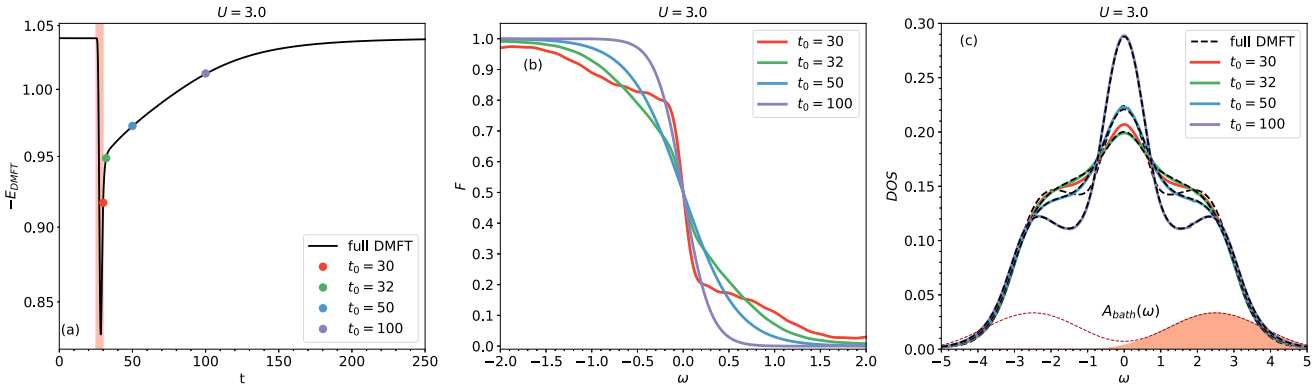

FIG. 1. (a) Energy $-E_{\mathrm{DMFT}}$ obtained from the full DMFT solution (interaction $U = 3$, initial inverse temperature $\beta = 20$, electron-phonon coupling $g^2 = 0.5$). Colored dots indicate the energies obtained from the auxiliary steady state $A_\omega^{\mathrm{NESS}}[F]$ [Eq. (66)], for different initial times t_0 at which the distribution functions $F(\omega, t_0)$ are taken from the DMFT solution and copied in the auxiliary steady-state problem. (b) Distribution functions $F(\omega, t_0)$ obtained from the full DMFT solution, at times t_0 corresponding to the dots in (a), and copied in the auxiliary steady-state problem. (c) Dashed lines show the spectrum $A(\omega, t_0)$ at various initial times, obtained from the full DMFT solution. Solid lines show the spectra obtained from the auxiliary steady state $A_\omega^{\mathrm{NESS}}[F]$ [Eq. (66)], evaluated with the distribution functions $F(\omega, t_0)$ in (b) taken from the DMFT solution. The dotted line at the bottom of (c) shows the (rescaled) spectral function $A_{\mathrm{bath}}(\omega)$ [Eq. (52)] for the excitation bath (the shaded orange area shows the occupied density of states for the bath), and the shaded area in (a) the time window over which this bath is coupled to the system.

B. Full DMFT solution

For the semielliptic density of states, the DMFT self-consistency can be formulated in closed form, and the hybridization of the impurity model is simply given by [32,33]

$$\Delta(t, t') = G(t, t') + \Gamma(t, t') \tag{57}$$

in terms of the local Green's function G. With the noninteracting Green's function of the impurity model [Eq. (42)], the Dyson equation for the impurity model reads as

$$G^{-1}(t, t') = \mathcal{G}^{-1}(t, t') - \Sigma_{\mathrm{int}}(t, t'). \tag{58}$$

Here

$$\Sigma_{\mathrm{int}}(t, t') = \Sigma_U(t, t') + \Sigma_{\mathrm{ph}}(t, t') \tag{59}$$

is the interaction self-energy due to the electron phonon interaction and the Hubbard interaction. The latter is determined using the iterated perturbation theory (IPT) impurity solver, i.e., a second-order expansion in terms of $\mathcal{G}$,

$$\Sigma_U(t, t') = U^2 \mathcal{G}(t, t')\mathcal{G}(t, t')\mathcal{G}(t', t). \tag{60}$$

In addition, the local energy $h(t)$ in Eq. (42) is the Hartree self-energy $h(t) = U n_\sigma(t)$ with the density $n_\sigma(t)$ per spin. In the present case we study a half-filled system, so that $\mu = U/2$ and $\mu + h(t) = 0$.

The IPT approximation is based on a second-order diagrammatic evaluation of the self-energy in terms of the Weiss field $\mathcal{G}$, that is the free impurity Green's function self-consistently determined in the DMFT iterations, rather than the bare noninteracting electron propagator. Viewed in terms of the bare Green's function, this corresponds to a nontrivial resummation of diagrams to infinite order. For this reason, the approximation turns out to be correct for the atomic limit of the half-filled Hubbard model in equilibrium [33], and thus provides a reasonable interpolation between the two exact limits $U = 0$ (metallic limit) and $t = 0$ (atomic limit). It qualitatively reproduces the DMFT equilibrium phase diagram of the half-filled Hubbard model and the Mott metal-insulator transition in the paramagnetic phase [33,61]. Quantitatively, deviations from quantum Monte Carlo (exact solver) start to appear in equilibrium around $U \approx 3$ in the weak-coupling regime [61]. For what concerns the nonequilibrium dynamics, the total energy is nicely conserved during the time evolution for values of $U \leqslant 3$ [61]. In this study, we therefore limit ourselves to $U \leqslant 3$, so that the expansion of the self-energy Σ in terms of the Weiss-field propagator $\mathcal{G}$ is appropriate both at equilibrium and in nonequilibrium.

The self-consistent solution of the system of Eqs. (57) to (60), together with the excitation and phonon self-energies (56) and (53), determines the time evolution of the physical system. The equations are solved on the Keldysh contour using the NESSi simulation package [38]. For the comparison with the QBE, the local spectral function and distribution function are then extracted from the Wigner transform of the local Green's function

$$A(\omega, t) = -\frac{1}{\pi}\mathrm{Im}G^R(\omega + i0, t), \tag{61}$$

$$F(\omega, t) = \frac{G^<(\omega, t)}{2\pi i A(\omega, t)}. \tag{62}$$

Furthermore, we compute the total energy as

$$E_{\mathrm{DMFT}} = -2i(\Delta * G)^<(t, t) - i(\Sigma_{\mathrm{int}} * G)^<(t, t). \tag{63}$$

The first and second terms represent the kinetic and interaction energy, respectively, with a factor 2 in the kinetic energy for the summation over spin components.

C. QBE formulation

For the present model, for which a closed set of equations is given in terms of local (momentum-averaged) quantities, the QBE can be derived directly for the local quantities. Instead of deriving Eqs. (28) and (29) from the lattice Dyson equation (25), one can perform an analogous argument directly for the

Dyson equation of the DMFT impurity model [Eq. (58)]. This leads to a local QBE

$$\partial_t F(\omega,t) = I[F(\cdot)], \tag{64}$$

$$\begin{aligned} I[F(\cdot)] = -i\{&[\Sigma^<(\omega,t)+\Delta^<(\omega,t)] \\ &+[\Sigma^R(\omega,t)+\Delta^R(\omega,t)]F(\omega,t) \\ &-F(\omega,t)[\Sigma^A(\omega,t)+\Delta^A(\omega,t)]\}, \end{aligned} \tag{65}$$

where again $\Sigma = \Gamma + \Sigma_{\rm int}$, and

$$\Sigma_{\rm int}(\omega,t) = \Sigma^{\rm NESS}_\omega[F(\cdot,t)],\ A(\omega,t) = A^{\rm NESS}_\omega[F(\cdot,t)], \tag{66}$$

$\Sigma(\omega,t)$, and the spectrum $A(\omega,t)$ are understood in terms of an auxiliary steady-state impurity model with given prescribed distribution function $\bar{F}(\omega) = F(\omega,t)$. The evaluation of these functionals is again done iteratively:

(1) Start from a guess for $\bar{\Sigma}_{\rm int}(\omega)$. Solve the steady-state variant of Eq. (58) for $\bar{G}^R(\omega)$,

$$\bar{G}^R(\omega) = \left[\omega+\mu-\bar{h}-\Delta^R(\omega)-\bar{\Sigma}^R_{\rm int}(\omega)\right]^{-1}, \tag{67}$$

and determine $\bar{A}(\omega) = -\frac{1}{\pi}\bar{G}^R(\omega+i0)$.

(2) Determine the lesser Green's function from the given distribution function $\bar{G}^<(\omega) = 2\pi i \bar{F}(\omega)\bar{A}(\omega)$.

(3) Use the self-consistency equation (57) to fix the hybridization function of the effective steady-state impurity model $\Delta(\omega) = \bar{G}(\omega) + \Gamma(\omega)$.

(4) Solve the impurity model. With IPT as an impurity solver, we first determine $\mathcal{G}(\omega)$ from $\Delta(\omega)$,

$$\mathcal{G}^R(\omega) = [\omega+\mu-h(t)-\Delta^R(\omega)]^{-1}, \tag{68}$$

$$\mathcal{G}^<(\omega) = \mathcal{G}^R(\omega)\Delta^<(\omega)\mathcal{G}^A(\omega), \tag{69}$$

transform to real time, evaluate Eq. (60), and transform back to frequency space to obtain $\Sigma^{R,<}_U(\omega)$. Similarly, $\Sigma^{R,<}_{\rm ph}(\omega)$ is evaluated.

(5) Set $\bar{\Sigma}_{\rm int}(\omega) = \Sigma_U(\omega) + \Sigma_{\rm ph}(\omega)$, and iterate steps (2)–(5) until convergence.

The iteration serves as a way to evaluate $\Sigma^{\rm NESS}[F(\cdot,t)]$. The differential equation (64) is then solved using a Runge-Kutta algorithm. In addition to the spectral and distribution functions, we then compute the total energy

$$E_{\rm QBE} = \frac{1}{2\pi}\int d\omega\{-2i[\Delta(\omega)G(\omega)]^< - i[\Sigma_{\rm int}(\omega)G(\omega)]^<\} \tag{70}$$

in order to compare with the full solution (63).

D. Results and discussion

In this section, we compare the QBE description with the full solution of the KB equations for the setting introduced in Sec. III A. Figure 1(a) shows the evolution of the energy in the full DMFT solution, which increases during the short excitation window, and subsequently relaxes back to the initial state due to electron thermalization and the electron-phonon interaction. Figures 1(b) and 1(c) then show the spectra and distribution functions at some points in time. In the initial and final states the spectrum has a central peak, representing a band of renormalized quasiparticles, which coexists with two Hubbard bands around $\omega = \pm U/2$. In equilibrium, with increasing T, the quasiparticle peak would be replaced by a dip in the spectral function, indicating that the high-temperature state is a bad metal without coherent quasiparticles. After the excitation, the distribution function is highly nonthermal, and the quasiparticle band is strongly suppressed. With time, $F(\omega,t)$ approaches back the shape of an approximate Fermi distribution (electron thermalization), and simultaneously the effective temperature of this distribution relaxes back to the initial $1/\beta$. Together with this evolution of the distribution function, the quasiparticle peak in the spectrum is reformed.

Before computing the time evolution generated by the QBE, we can independently evaluate the quality of the auxiliary steady-state representation of the spectra at each given time, i.e., the accuracy of the functional $A^{\rm NESS}_\omega[F]$ [Eq. (66)]: We take the distribution function $F(\omega,t_0)$ from the full solution at a given time t_0, evaluate $A^{\rm NESS}_\omega[\bar{F}]$ with $\bar{F}(\omega) = F(\omega,t_0)$ as described below Eq. (66) to compute a steady-state spectrum $\bar{A}(\omega)$, and compare the result with the full solution $A(\omega,t_0)$. In Fig. 1(c), dashed lines correspond to the DMFT solution $A(\omega,t_0)$, while solid lines show the corresponding $\bar{A}(\omega)$. The comparison is perfect, even for relatively early times. Only for times immediately after the ultrafast excitation ($t = 30$), where the gradient approximation is not supposed to work, can one observe a failure of the auxiliary steady-state representation. We can therefore affirm that the density of states can be very accurately obtained as a steady-state functional of the distribution function, even in the correlated metallic regime. For smaller values of U, the agreement is as good (not shown here). We note that, in the context of strongly correlated systems, we have concentrated here on the weak-to-intermediate coupling $U \lessapprox U_c/2$, with U_c the critical value for the Mott transition in the paramagnetic phase. The scattering integral evaluated by IPT (or DMFT plus weak-coupling expansion) is, however, already significantly different from the bare perturbation theory, and particularly contains the information of the Mott metal-insulator transition. Furthermore, not only the density of states can be very accurately obtained as a steady-state functional of the distribution function, but the whole Green's function and self-energy: The energy values represented by colored dots in Fig. 1(a), calculated with Eq. (70), exactly match the ones of the full DMFT code at the same time, calculated with Eq. (63).

In passing, we note that a nonequilibrium spectral function $A(\omega,t)$ defined by the Wigner transform (12) is real (Hermitian) by construction, but not necessarily positive, while a steady-state fermionic spectral function is always positive. Moreover, for numerical reasons, for short times the integral in the Wigner transform (12) is truncated, possibly leading to small artifacts. In practice, the relation $F(\omega,t) = \bar{F}(\omega)$ will therefore not be enforced exactly, but as a best fit. It should be noted, however, that the positivity of $A(\omega,t)$ and $F(\omega,t)$ is indeed satisfied wherever the gradient approximation is accurate, as discussed in connection with Eq. (18). In particular, as one can see from Fig. 1(b), the distribution functions are already positive in the relevant time interval for the present case.

Next, we compare the relaxation dynamics of the system in the two descriptions. For this, we simply take the distribution function $F(\omega,t_0)$ at a given time t_0 from the full DMFT

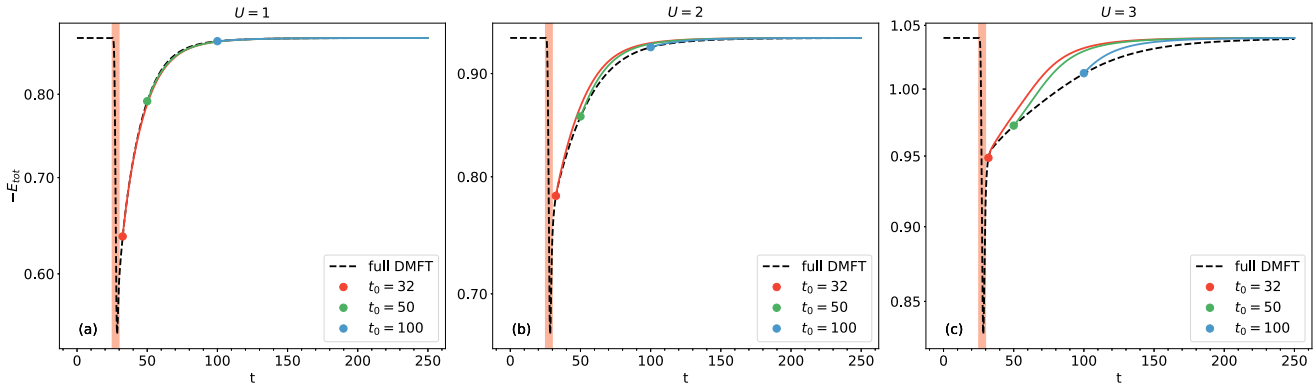

FIG. 2. Time evolution of the total energy for $U = 1$ (a), $U = 2$ (b), and $U = 3$ (c) (initial inverse temperature $\beta = 20$, electron-phonon coupling $g^2 = 0.5$). The black dashed lines show the energy $-E_{\mathrm{DMFT}}$ obtained from the full DMFT evolution, solid lines show the energy $-E_{\mathrm{QBE}}$ obtained from the QBE. The QBE is started at different times t_0 (indicated by the dots at the beginning of the dashed lines), taking the distribution function $F_{\mathrm{DMFT}}(\omega, t_0)$ as an initial state for a solution of the QBE at times $t > t_0$.

solution as an initial state for a solution of the QBE for $t > t_0$. The time evolution of the energy is shown in Fig. 2 for three different values of U, and different starting times t_0 of the QBE simulation. For small values of U [$U = 1$ and 2 in Figs. 2(a) and 2(b), respectively], the energy relaxation rate obtained from the QBE is almost identical to the one from full DMFT. For $U = 3$ [Fig. 2(c)], one can observe a difference in the magnitude of the time constants related to the relaxation of the total energy in the two approaches. In particular, the QBE presents an artificially faster relaxation with respect to the full DMFT solution. This indicates that the gradient approximation is less justified for $U = 3$, which could be related to the existence of a more narrow quasiparticle band. As the starting point t_0 of the Boltzmann code shifts forward in time, the difference between the time evolution of the energies becomes less pronounced. If one decreases the coupling g^2 with the phonon bath (not shown), the relaxation dynamics of the system is slowed down, the gradient approximation is more justified, and the difference in the energy relaxation rate in the two approaches is less pronounced.

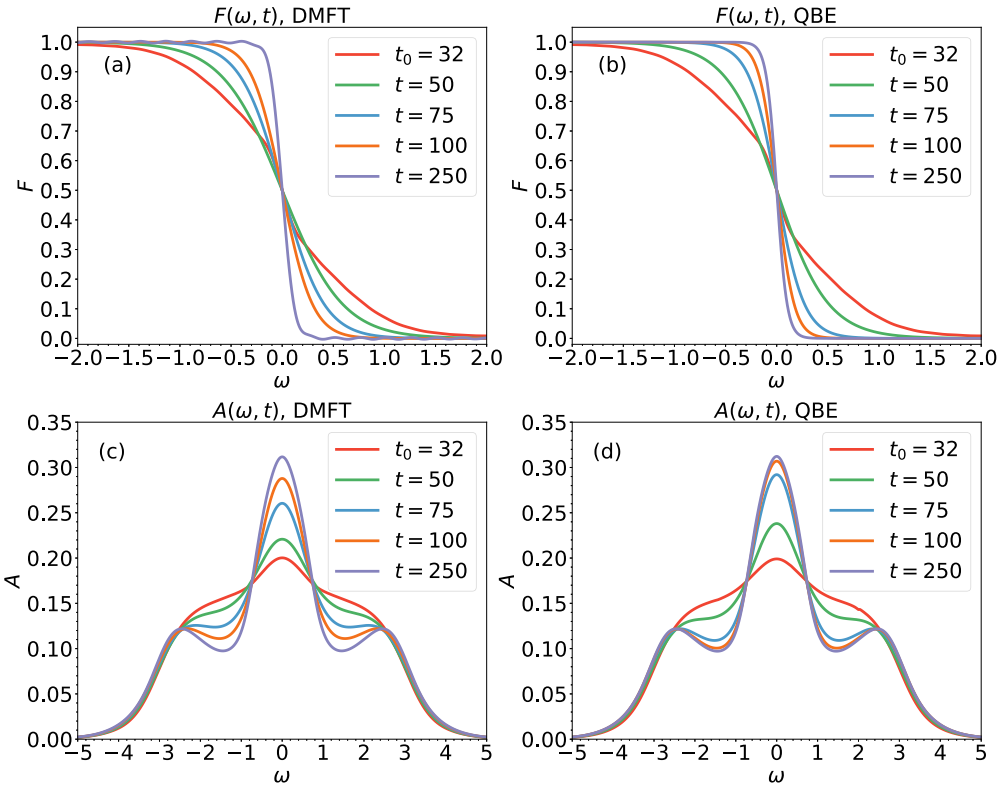

FIG. 3. Distribution function (upper panels) and spectral function (lower panels) obtained from the full DMFT solution (left panels) and the QBE (right panels) one at $U = 3$. The QBE takes the DMFT distribution function $F(\omega, t_0)$ at time $t_0 = 32$ as initial state for the evolution at $t > t_0$ (initial inverse temperature $\beta = 20$, electron phonon coupling $g^2 = 0.5$).

Although the relaxation rate for the energy in the QBE seems to be overestimated for larger values of U, Fig. 3 shows that the spectra and distribution functions obtained from the full DMFT and the QBE follow the same qualitative behavior, i.e., a relaxation of $F(\omega, t)$ to a Fermi function together with an evolution of the temperature in this Fermi function towards the initial temperature.

IV. CONCLUSION

In conclusion, we developed a kinetic equation which works without the need to assume the existence of quasiparticles with well-defined dispersion $\epsilon_{\boldsymbol{k}}$ and, above all, evaluates the scattering integral in a nonperturbative manner. In particular, a scattering integral which is consistent with DMFT is obtained by extracting self-energies from a quantum impurity model in an auxiliary nonequilibrium steady state. Most importantly, this guarantees that the final state of the evolution is a proper description of the fully interacting state of the correlated electron system. This makes the present formalism unique with respect to conventional quantum kinetic approaches based on perturbative scattering integrals or certain assumptions on the spectral function, such as the rigidity of density of states during the time evolution, or the quasiparticle approximation. While for full nonequilibrium Green's function simulations the numerical effort for the propagation over a time interval $t_{\max}$ scales with $O(t_{\max}^3)$, and the required memory scales with $O(t_{\max}^2)$, in the QBE the numerical effort is linear with $t_{\max}$ and the memory required is independent of $t_{\max}$.

We have tested the framework on the relaxation of the electronic state in a correlated metal after a population transfer that simulates a photoexcitation. One assumption of the QBE, i.e., that the spectra at the correlated system can be obtained from an auxiliary steady state, is found to be satisfied with remarkable accuracy. Moreover, the relaxation dynamics for both spectral functions and distribution functions within the full nonequilibrium DMFT simulation and the QBE are consistent. Quantitatively, the gradient approximation underlying the QBE leads to a slight overestimation of the relaxation rate. Whether this can be corrected by higher-order expansions of the gradient approximation is left for future investigations.

The success of the QBE approach for the present setting motivates an application to different models. In particular, this includes symmetry-broken states where interesting long-time phenomena have been observed [62], and the evolution of the Mott phase, where already a QBE with an *ad hoc* scattering integral has shown relative success [42]. Possible applications of the formalism include the evolution of the density of states in correlated systems, in particular multiorbital systems where a pronounced effect of the redistribution of weight has already been discussed using quasiparticle kinetic equations [63]. In this context, the method can be combined with *GW* [6] or DMFT+*GW* [64], which have demonstrated again a pronounced dependence of the spectra on the distribution. In general, the QBE is potentially most efficient in situations which naturally have a large separation of timescales. Examples include the coupled electron lattice dynamics, and the evolution of "photodoped" systems, in which some electronic variables (in particular the occupation of different Hubbard subbands) evolve on the picosecond timescale. The resulting states may be described as quasisteady states, where these slow variables become quasithermodynamic quantities which determine new phases like excitonic order and superconductivity. For example, a quasi-steady-state approach has recently been used to explore η-pairing superconductivity in the photodoped Hubbard model [49,65]. The QBE provides the leading correction to such a quasisteady approach, and allows to determine the lifetime or potential metastability of such long-lived states. Finally, another interesting perspective of the approach is that there are several promising numerical approaches to study nonequilibrium steady states within DMFT. This includes variants of the strong-coupling expansion [66,67], matrix product states [68], auxiliary master equations [69], or quantum Monte Carlo [70,71]. The QBE formalism would allow these nonperturbative techniques to access not only true steady states, but also nonequilibrium states of correlated electrons on the picosecond timescale relevant for photoinduced phase transition and collective orders.

ACKNOWLEDGMENTS

We acknowledge P. Werner for useful discussions, and N. Dasari for discussions as well as his contribution to the implementation of the Ohmic bath. This work was supported by the ERC Starting Grant No. 716648. The calculations have been done at the RRZE of the University Erlangen-Nuremberg.

[1] D. N. Basov, R. D. Averitt, and D. Hsieh, Nat. Mater. **16**, 1077 (2017).

[2] C. Giannetti, M. Capone, D. Fausti, M. Fabrizio, F. Parmigiani, and D. Mihailovic, Adv. Phys. **65**, 58 (2016).

[3] H. Ichikawa, S. Nozawa, T. Sato, A. Tomita, K. Ichiyanagi, M. Chollet, L. Guerin, N. Dean, A. Cavalleri, S.-i. Adachi, T.-h. Arima, H. Sawa, Y. Ogimoto, M. Nakamura, R. Tamaki, K. Miyano, and S.-y. Koshihara, Nat. Mater. **10**, 101 (2011).

[4] D. Fausti, R. I. Tobey, N. Dean, S. Kaiser, A. Dienst, M. C. Hoffmann, S. Pyon, T. Takayama, H. Takagi, and A. Cavalleri, Science (New York, N.Y.) **331**, 189 (2011).

[5] P. Beaud, A. Caviezel, S. O. Mariager, L. Rettig, G. Ingold, C. Dornes, S.-W. Huang, J. A. Johnson, M. Radovic, T. Huber, T. Kubacka, A. Ferrer, H. T. Lemke, M. Chollet, D. Zhu, J. M. Glownia, M. Sikorski, A. Robert, H. Wadati, M. Nakamura *et al.*, Nat. Mater. **13**, 923 (2014).

[6] D. Wegkamp, M. Herzog, L. Xian, M. Gatti, P. Cudazzo, C. L. McGahan, R. E. Marvel, R. F. Haglund, A. Rubio, M. Wolf, and J. Stähler, Phys. Rev. Lett. **113**, 216401 (2014).

[7] L. Stojchevska, I. Vaskivskyi, T. Mertelj, P. Kusar, D. Svetin, S. Brazovskii, and D. Mihailovic, Science **344**, 177 (2014).

[8] S. Mor, M. Herzog, D. Golež, P. Werner, M. Eckstein, N. Katayama, M. Nohara, H. Takagi, T. Mizokawa, C. Monney, and J. Stähler, Phys. Rev. Lett. **119**, 086401 (2017).

[9] M. Budden, T. Gebert, M. Buzzi, G. Jotzu, E. Wang, T. Matsuyama, G. Meier, Y. Laplace, D. Pontiroli, M. Riccò *et al.*, Nat. Phys. **17**, 611 (2021).

[10] A. Polkovnikov, K. Sengupta, A. Silva, and M. Vengalattore, Rev. Mod. Phys. **83**, 863 (2011).

[11] J. Berges, S. Borsányi, and C. Wetterich, Phys. Rev. Lett. **93**, 142002 (2004).

[12] M. Moeckel and S. Kehrein, Phys. Rev. Lett. **100**, 175702 (2008).

[13] M. Kollar, F. A. Wolf, and M. Eckstein, Phys. Rev. B **84**, 054304 (2011).

[14] T. Langen, T. Gasenzer, and J. Schmiedmayer, J. Stat. Mech.: Theory Exp. (2016) 064009.

[15] L. P. Kadanoff and G. Baym, *Quantum Statistical Mechanics: Green's Function Methods in Equilibrium and Nonequilibrium Problems* (CRC Press, Boca Raton, FL, 1962).

[16] A. Kamenev, *Field Theory of Non-Equilibrium Systems* (Cambridge University Press, Cambridge, 2011).

[17] M. Bonitz, *Quantum Kinetic Theory* (Springer International Publishing AG Switzerland, 1998).

[18] D. Kremp, M. Bonitz, W. Kraeft, and M. Schlanges, Ann. Phys. **258**, 320 (1997).

[19] F. Queisser and R. Schützhold, Phys. Rev. A **100**, 053617 (2019).

[20] H. Haug and A.-P. Jauho, *Quantum Kinetics in Transport and Optics of Semiconductors* (Springer, Berlin, 2008).

[21] A. Georges, L. d. Medici, and J. Mravlje, Annu. Rev. Condens. Matter Phys. **4**, 137 (2013).

[22] X. Deng, J. Mravlje, R. Žitko, M. Ferrero, G. Kotliar, and A. Georges, Phys. Rev. Lett. **110**, 086401 (2013).

[23] M. Eckstein and P. Werner, Phys. Rev. Lett. **110**, 126401 (2013).

[24] S. Sayyad and M. Eckstein, Phys. Rev. Lett. **117**, 096403 (2016).

[25] N. Dasari, J. Li, P. Werner, and M. Eckstein, Phys. Rev. B **103**, L201116 (2021).

[26] J. C. Petersen, A. Farahani, D. G. Sahota, R. Liang, and J. S. Dodge, Phys. Rev. B **96**, 115133 (2017).

[27] D. G. Sahota, R. Liang, M. Dion, P. Fournier, H. A. Dabkowska, G. M. Luke, and J. S. Dodge, Phys. Rev. Res. **1**, 033214 (2019).

[28] D. Golež, P. Werner, and M. Eckstein, Phys. Rev. B **94**, 035121 (2016).

[29] M. Babadi, E. Demler, and M. Knap, Phys. Rev. X **5**, 041005 (2015).

[30] J. D. Rameau, S. Freutel, A. F. Kemper, M. A. Sentef, J. K. Freericks, I. Avigo, M. Ligges, L. Rettig, Y. Yoshida, H. Eisaki, J. Schneeloch, R. D. Zhong, Z. J. Xu, G. D. Gu, P. D. Johnson, and U. Bovensiepen, Nat. Commun. **7**, 13761 (2016).

[31] N. Schlünzen, J.-P. Joost, F. Heidrich-Meisner, and M. Bonitz, Phys. Rev. B **95**, 165139 (2017).

[32] H. Aoki, N. Tsuji, M. Eckstein, M. Kollar, T. Oka, and P. Werner, Rev. Mod. Phys. **86**, 779 (2014).

[33] A. Georges, G. Kotliar, W. Krauth, and M. J. Rozenberg, Rev. Mod. Phys. **68**, 13 (1996).

[34] P. Lipavský, V. Špička, and B. Velický, Phys. Rev. B **34**, 6933 (1986).

[35] N. Schlünzen, J.-P. Joost, and M. Bonitz, Phys. Rev. Lett. **124**, 076601 (2020).

[36] M. Schüler, J. C. Budich, and P. Werner, Phys. Rev. B **100**, 041101(R) (2019).

[37] Y. Murakami, M. Schüler, S. Takayoshi, and P. Werner, Phys. Rev. B **101**, 035203 (2020).

[38] M. Schüler, U. De Giovannini, H. Hübener, A. Rubio, M. A. Sentef, T. P. Devereaux, and P. Werner, Phys. Rev. X **10**, 041013 (2020).

[39] E. Perfetto and G. Stefanucci, J. Phys.: Condens. Matter **30**, 465901 (2018).

[40] M. Schüler, M. Eckstein, and P. Werner, Phys. Rev. B **97**, 245129 (2018).

[41] J. Kaye and D. Golež, SciPost Phys. **10**. 91 (2021).

[42] M. Wais, M. Eckstein, R. Fischer, P. Werner, M. Battiato, and K. Held, Phys. Rev. B **98**, 134312 (2018).

[43] M. Wais, J. Kaufmann, M. Battiato, and K. Held, Phys. Rev. B **103**, 205141 (2021).

[44] A. V. Joura, J. K. Freericks, and T. Pruschke, Phys. Rev. Lett. **101**, 196401 (2008).

[45] J. Li, C. Aron, G. Kotliar, and J. E. Han, Phys. Rev. Lett. **114**, 226403 (2015).

[46] I. Titvinidze, M. E. Sorantin, A. Dorda, W. von der Linden, and E. Arrigoni, Phys. Rev. B **98**, 035146 (2018).

[47] A. Matthies, J. Li, and M. Eckstein, Phys. Rev. B **98**, 180502(R) (2018).

[48] O. Scarlatella, A. A. Clerk, R. Fazio, and M. Schirò, Phys. Rev. X **11**, 031018 (2021).

[49] J. Li, D. Golez, P. Werner, and M. Eckstein, Phys. Rev. B **102**, 165136 (2020).

[50] J. Panas, M. Pasek, A. Dhar, T. Qin, A. Geißler, M. Hafez-Torbati, M. E. Sorantin, I. Titvinidze, and W. Hofstetter, Phys. Rev. B **99**, 115125 (2019).

[51] J. K. Freericks, H. R. Krishnamurthy, and T. Pruschke, Phys. Rev. Lett. **102**, 136401 (2009).

[52] M. Eckstein and M. Kollar, Phys. Rev. B **78**, 245113 (2008).

[53] N. Tsuji, T. Oka, and H. Aoki, Phys. Rev. Lett. **103**, 047403 (2009).

[54] M. Büttiker, Phys. Rev. B **32**, 1846 (1985).

[55] J. M. Luttinger and J. C. Ward, Phys. Rev. **118**, 1417 (1960).

[56] G. Baym and L. P. Kadanoff, Phys. Rev. **124**, 287 (1961).

[57] M. Potthoff, Eur. Phys. J. B **32**, 429 (2003).

[58] E. Kozik, M. Ferrero, and A. Georges, Phys. Rev. Lett. **114**, 156402 (2015).

[59] T. Schäfer, G. Rohringer, O. Gunnarsson, S. Ciuchi, G. Sangiovanni, and A. Toschi, Phys. Rev. Lett. **110**, 246405 (2013).

[60] M. Eckstein, M. Kollar, and P. Werner, Phys. Rev. Lett. **103**, 056403 (2009).

[61] N. Tsuji and P. Werner, Phys. Rev. B **88**, 165115 (2013).

[62] A. Picano and M. Eckstein, Phys. Rev. B **103**, 165118 (2021).

[63] Z. He and A. J. Millis, Phys. Rev. B **93**, 115126 (2016).

[64] D. Golež, L. Boehnke, M. Eckstein, and P. Werner, Phys. Rev. B **100**, 041111(R) (2019).

[65] Y. Murakami, S. Takayoshi, T. Kaneko, Z. Sun, D. Golež, A. J. Millis, and P. Werner, arXiv:2105.13560v1.

[66] O. Scarlatella and M. Schirò, arXiv:1904.07679.

[67] J. Li and M. Eckstein, Phys. Rev. B **103**, 045133 (2021).

[68] F. Schwarz, I. Weymann, J. von Delft, and A. Weichselbaum, Phys. Rev. Lett. **121**, 137702 (2018).

[69] E. Arrigoni, M. Knap, and W. von der Linden, Phys. Rev. Lett. **110**, 086403 (2013).

[70] R. E. V. Profumo, C. Groth, L. Messio, O. Parcollet, and X. Waintal, Phys. Rev. B **91**, 245154 (2015).

[71] C. Bertrand, S. Florens, O. Parcollet, and X. Waintal, Phys. Rev. X **9**, 041008 (2019).